Available online at www.sciencedirect.com
ScienceDirect
Journal of the European Ceramic Society 29 (2009) 1077–1082
www.elsevier.com/locate/jeurceramsoc

Microstructure and mechanical properties of an alumina–glass low temperature co-fired ceramic

Yang-Fei Zhang [a], Shu-Lin Bai [a,*], Min Miao [b,c], Yu-Feng Jin [b]

[a] *LTCS, Department of Advanced Materials and Nanotechnology, College of Engineering, Peking University, Beijing 100871, China*
[b] *National Key Laboratory on Micro/Nano Fabrication Technology, Peking University, Beijing 100871, China*
[c] *Information Microsystem Research Institute, Beijing Information Technology Institute, Beijing 100101, China*

Received 24 April 2008; received in revised form 30 July 2008; accepted 30 July 2008
Available online 9 September 2008

Abstract

The microstructure and mechanical properties of an alumina–glass low temperature co-fired ceramic (LTCC) have been investigated. The microstructure was studied by using optical microscope, scanning electron microscope, energy spectrum analysis and X-ray diffraction. The Young's modulus, hardness, flexure strength and fracture toughness were measured by three-point bending, indentation and nanoindentation tests. The LTCC can be regarded as a particle-reinforced composite with macroscopically isotropic properties: particles mainly composed of synthetic corundum and matrix mainly of corundum and silica. The particles with irregular shape and an average radius of 0.71 μm are homogeneously dispersed in the matrix. The properties of the individual particle and matrix were successfully measured and further used to obtain the effective properties of the composite by micromechanics methods. The existence of rigid particles improves not only the modulus, hardness and strength but also the fracture toughness of LTCC materials.

Keywords: Microstructure; Mechanical properties; LTCC; Sintering; Al_2O_3

1. Introduction

Low temperature co-fired ceramic (LTCC) is a newly developed material widely used in microelectronics packaging, multi-chip-model (MCM) and system-in-package (SiP) applications. The advantages of LTCC include: utilizing highly conductive metals, low dielectric constant, high quality factor (Q value), low sintering temperature, high print resolution of conductors, low surface roughness, high layer count, small temperature coefficient of expansion, easy to fabricate and inexpensive to process. The early material developed for hybrid electronic packages was thick film, and then high temperature co-fired ceramic (HTCC) was developed to deal with the new challenges of packaging, multilayer MCM and interfacing with meso-scale devices and three-dimensional (3D) structures.[1,2] The high sintering temperature enhances the condition of fabrication and limits the kinds of conductive metals, so LTCC technology was developed to reduce the temperature lower than 1000 °C. LTCC is in practice a glass–ceramic composite which crystallizes at optimized processing parameters.[3,4] The ceramic fillers extensively used are alumina, high thermal conductive berillia, ferroelectric perovskite, ferromagnetic spinel and photovoltaic–piezoelectric ceramics. While the typical glass systems are borosilicate, lead borosilicate, sodium borosilicate, etc. Alumina–glass composites are advanced systems with suitable chemical, electrical and mechanical properties and some of them have been fabricated to commercially available green tapes such as Dupont 951 AT.[5,6]

LTCC provides a convenient medium for fabricating laminated structures where the internal 3D channels and cavities can be served for heat dissipation and manufacturing or embedding various sensors into microsystem-level-packages including inertia measurement unit, fluid flow detector, hybrid micro-valve and micro-pump.[1,7] Many LTCC integrated devices have to operate under harsh environmental conditions where the mechanical stress is a critical issue regarding the reliability of the devices. The prediction of the lifetime and failure rate of LTCC can be achieved by investigating the mechanical properties.[8] The study

* Corresponding author. Tel.: +86 10 6275 3328; fax: +86 10 6275 7563.
E-mail address: slbai@pku.edu.cn (S.-L. Bai).

0955-2219/$ – see front matter © 2008 Elsevier Ltd. All rights reserved.
doi:10.1016/j.jeurceramsoc.2008.07.056

on the microstructure and mechanical properties was carried out and the results may be valuable in the improvement of the LTCC design.[9–14] Jones et al.[6] have studied the chemical, structural and mechanical properties of six commercially available LTCC materials based on different devitrifying glass–ceramic systems, including wollenstite, anorthite and celsian phases with ceramic modifiers of alumina. Moreover, Lu and Qiu[15] have investigated the effect of borosilicate glass and firing temperature on the microstructure and properties of the glass–ceramic composites. Most of previous works are based on the assumption that LTCC is a single-phase isotropic material. However, in some situations such as the generation and propagation of the micro-cracks, the heterogeneity of microstructures plays a key role. In this case, one has to take into account of the effect of filler size and dispersion on the mechanical properties. With the development of high resolution nanoindentation testing instruments, the individual characterization of each phase in LTCC becomes possible and accurate.

The objective of the present work is to investigate the microstructure and mechanical properties, as well as their relationship of a high performance LTCC. Several experimental methods including nano-, micro- and macro-tests are used to characterize the microstructure and mechanical properties of LTCC. The results obtained are helpful to the reliability study of LTCC based microelectronic devices, as well as the optimization of material synthesis and processing parameters.

2. Experimental

The material studied is a commercially available green tape: DuPont 951 AT with single layer height of $114 \pm 8\,\mu m$. This tape is a Pb–borosilicate glass filled with alumina particles[16]. The plates were laminated with 11 layers and vacuum sintered at 70 °C for 10 min, then 400 °C for 20 min, and finally 850 °C for another 20 min. The sintered plates with dimension of 140 mm × 140 mm × 1.02 mm were laser cut into samples for mechanical tests with the geometry shown in Fig. 1. Residual stress, thermal deformation and breaking easily caused by other cutting methods for brittle, high melting point and hard materials can be avoided. In addition, the laser cutting provides a smooth and crack-free cut plane, a small heat-affected zone and a small material deformation. The top and lateral faces of the samples were polished with emery papers in discrete steps down to a 2000 grade finish. The face roughness after polishing was decreased from 210 nm Ra (roughness average) to 36 nm Ra, measured by a scanning probe microscope (SPM) of TriboIndenter (Hysitron Co.) in contact mode on a scan area of 60 μm × 60 μm.

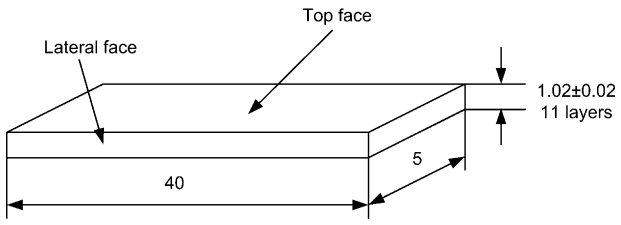

Fig. 1. Sample geometry for mechanical tests (dimension in mm).

The three-point bending (3PB) tests were performed on Instron 3365 by following the international standard ISO 14704 with the span of 30 mm. A low loading rate of 0.05 mm/min was particularly chosen in order to control easily the test process and obtain the accurate recording data.

The indentation tests were carried out on the polished top face by using MVK-H210 (Akashi Co.) with a standard Vickers diamond tip. The loading rate was 1 N/s and the values of load applied were 5, 10 and 20 N, respectively. The fracture toughness was then calculated with the equation adopted as[17]:

$$K_{IC} = 5.1636 H a^2 c^{-1.5} \quad (1)$$

where H is the hardness, a is the average half length of the diagonals of indent pit and c is the average length of four cracks extending from the indent pit.

Furthermore, the nanoindentation tests were undertaken on TriboIndenter with a Berkovich diamond tip of a nominal radius of curvature equal to ~100 nm. The maximum load was 9 mN. Twenty indents were made to obtain average values of the Young's modulus and hardness. During the experiments, the temperature was controlled at ~26 °C and the relative humidity at ~43%. To get the Young's modulus of both particle and matrix, the modulus mapping was performed using a nano-DMA II^{TM} adjunct of the TriboIndenter with nano-scale lateral resolution.

The microstructure was investigated under optical microscope (OM) (BX51M, Olympus Co.), scanning electron microscope (SEM) (Quanta 200FEG, FEI Co.) equipped with energy dispersive X-ray (EDX) detector and X-ray diffraction (XRD) (X' Pert Pro, Panalytica Co.).

3. Results and discussion

3.1. Microstructure and composition of LTCC studied

By SEM observation on the top face of LTCC samples, the LTCC material is found to be composed of two phases: dispersed particles and continuous matrix, as shown in Fig. 2a. The particles with irregular shape and different size are randomly distributed in the matrix. Detailed examination of the particle phase shows the existence of the "salami" structure, i.e., there is some matrix phase inside the large particles, judged from the identical grey color of the phase with the matrix. When sintering, the fluid matrix phase enveloped initially by the small particles possibly solidifies simultaneously with the agglomeration of small particles into large ones. Therefore, the co-existence of particle phase and matrix phase after the sintering engenders the "salami" structure. This type of microstructure was also observed by other authors[11,18]. The micrograph taken on the lateral fracture surface under low magnification in Fig. 2b shows that the pile interface or boundary of initial 11 layers disappears after the sintering process, which signifies that the LTCC studied is well solidified.

If the particle shape is assumed to be ball-like and by using the technique of image treatment, the radius of particles is found to be from several hundred nanometers to tens micrometers.

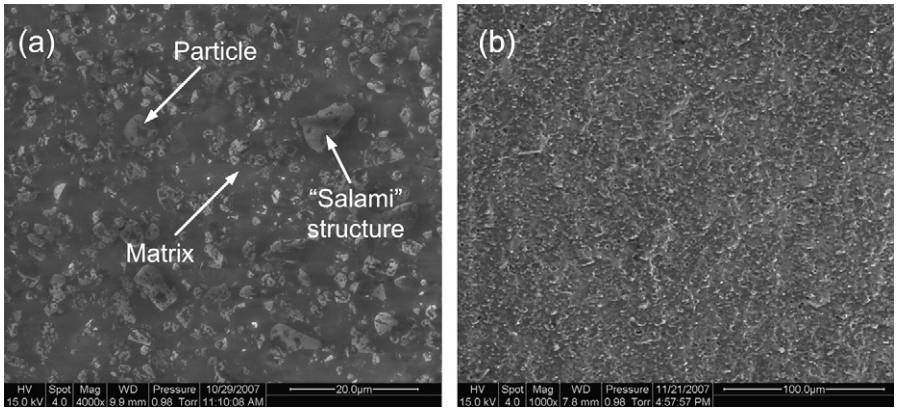

Fig. 2. SEM photographs of LTCC (a) top face with high resolution and (b) fracture surface with low resolution.

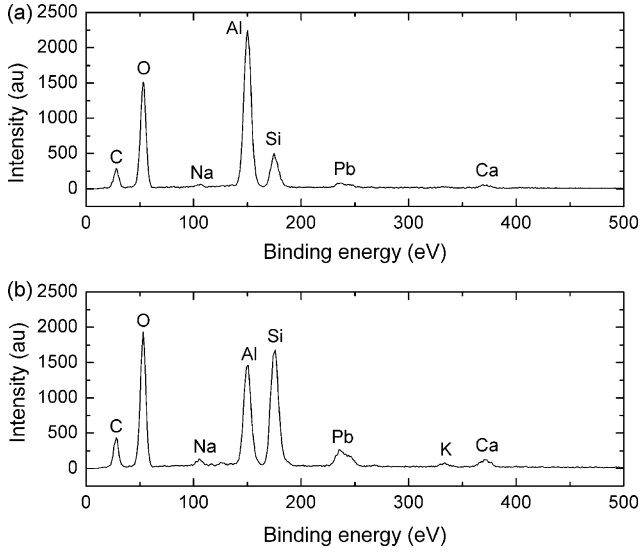

Fig. 3. EDX analysis on (a) the particle and (b) the matrix.

The average radius calculated from 3151 particles is 0.71 μm and the volume fraction of particles is about 27%. From the measurement by EDX, as shown in Fig. 3, the Al content in the particle is higher than that in the matrix. However, the Si and O content is inversed. By XRD measurement, it is found that the particle is mainly composed of Al_2O_3 and the matrix mainly of Al_2O_3 and SiO_2.

3.2. Mechanical properties

3.2.1. Nanoindentation tests

Fig. 4 shows the Young's modulus and hardness of LTCC samples as a function of penetration depth, measured by nanoindentation tests. The scatter of the points indicates a range of values of Young's modulus and hardness, not simply the discrete values corresponding to the matrix and the particles. This is related to the microstructure of the LTCC, as well as large particles, many tiny particles are also embedded in the matrix. So the real response of the LTCC to the indentation force comes from the combination effect of both matrix and those tiny particles. If the indenter tip is pressed on the location where the particle density is high, the penetration depth is small and the value of modulus and hardness is large. Otherwise, the modulus and hardness are small. The dispersion and content of tiny particles may locally change place by place because of the heterogeneity of microstructure, this causes the continuous change of modulus and hardness measured with the penetration depth. It must be indicated that the maximum and minimum values in Fig. 4 correspond to the properties of particles and pure matrix, respectively.

Another method with nanoindentation tests, the modulus mapping, was particularly adopted for the modulus measurement of each phase in the multiphase materials. In Fig. 5 is shown the modulus mapping image on an area of 15 μm × 15 μm consisted of 256 × 256 points. The 3D profile image in Fig. 5a was obtained by monitoring the indenter tip displacement. In Fig. 5b, different colors represent different modulus values, from which the modulus of the particle is much larger than that of the matrix. Additionally, the measurement along the black line in Fig. 5b is made, which distinctly and quantitatively reveals the variation of the modulus across the particles and the matrix, as shown in Fig. 5c. The moduli are about 200 and 80 GPa for particles and matrix, respectively. The measured modulus of particles is smaller than that of high-purity Al_2O_3. The main reason is the presence of SiO_2 in the particle, which is revealed by the EDX measurement. The modulus of SiO_2 is much smaller than that of Al_2O_3, so the modulus measured of particles containing both Al_2O_3 and SiO_2 in this work is much smaller than that of pure Al_2O_3 given in literature. Another reason is alike the effect of substrate rigidity on the nanoindentation measurement for multilayer films. The particle is embedded in the low modulus matrix which serves as a soft substrate. When the indentation is applied on the particle–matrix assemblage, the soft matrix "substrate" will cushion the force and so reduce the rigidity of hard particle "surface layer". By comparing the maximum and minimum values of modulus in Fig. 4a with Fig. 5c, the measurements by nanoindentation and modulus mapping give the same results.

3.2.2. Three-point bending tests and comparison with theoretical prediction

By the 3PB tests, the modulus measured of LTCC material is 114.88 ± 0.98 GPa, which agrees well with the four-point bending test result of 120 GPa supplied by Dupont Company. The flexural strength is 201.80 ± 6.43 MPa. Due to

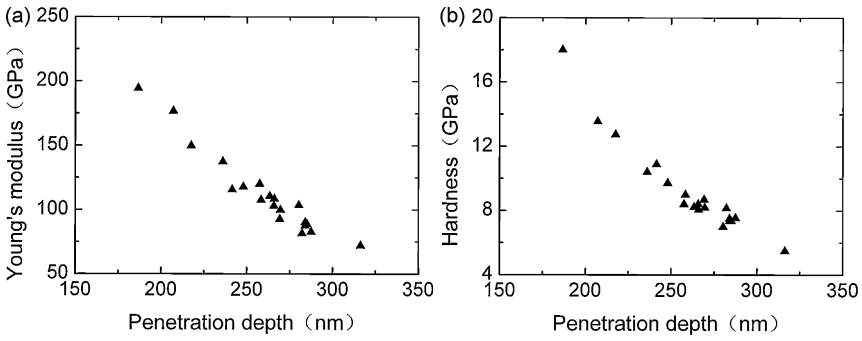

Fig. 4. (a) Young's modulus and (b) hardness vs penetration depth on top face.

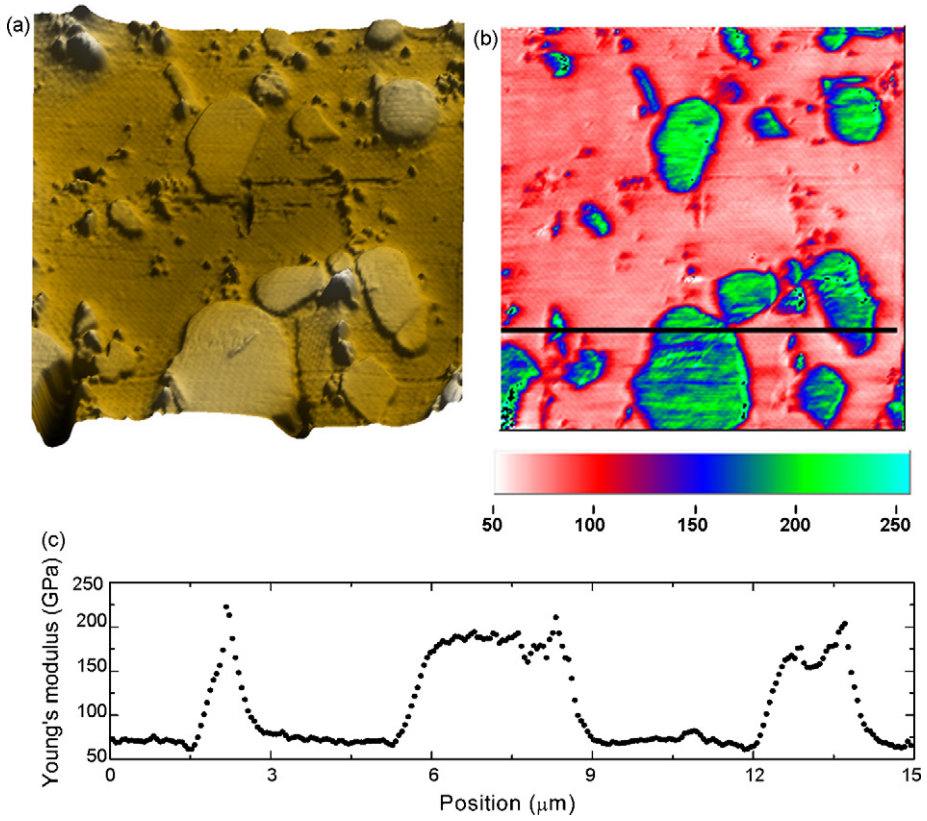

Fig. 5. (a) 3D SPM, (b) modulus mapping photograph of top face on a scan area of 15 μm × 15 μm and (c) modulus distribution along the black line in (b).

the brittleness of LTCC, the load–deflection curve is linear until final failure. In calculating the average value of moduli given in Fig. 4a, we have the modulus equal to 116.21 GPa, which is very close to that by 3PB tests. It should be indicated that the laser cutting left no defects on the lateral face, so bending results are reliable.

In order to predict theoretically the modulus of LTCC, the micromechanics model developed by Weng[19] based on Mori–Tanaka method is used. Besides, the rule of mixtures is also used with the advantage of ignoring the shape and size of the particle and Poisson's ratio of each phase. The effective Young's modulus is calculated by Eqs. (2)–(4) of Mori–Tanaka method and Eq. (5) of the rule of mixtures:

$$\frac{k_c}{k_0} = 1 + \frac{V_1(k_1 - k_0)}{k_0 + (1 - V_1)\left[(k_1 - k_0)/(k_0 + 4\mu_0/3)\right] k_0} \tag{2}$$

$$\frac{\mu_c}{\mu_0} = 1 + \frac{V_1(\mu_1 - \mu_0)}{\mu_0 + (1 - V_1)(\mu_1 - \mu_0)/\{1 + (9k_0 + 8\mu_0)/[6(k_0 + 2\mu_0)]\}} \tag{3}$$

$$k = \frac{E}{3(1 - 2v)}, \qquad \mu = \frac{E}{2(1 + v)} \tag{4}$$

$$E_c = E_1 V_1 + E_0(1 - V_1) \tag{5}$$

where E, k, μ, v and V are Young's modulus, bulk modulus, shear modulus, Poisson's ratio and volume fraction, respectively, and the subscripts 0, 1, c represent matrix, particle and composite, respectively. With the moduli of particle and matrix obtained from modulus mapping measurements, the calculated

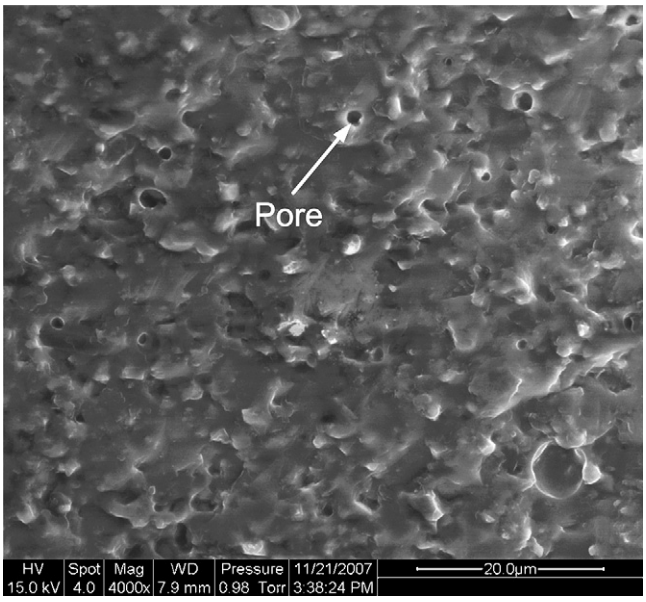

Fig. 6. Micrograph of fracture surface by three-point bending tests.

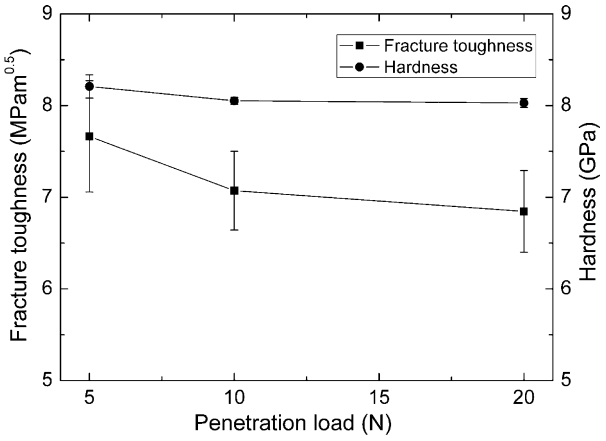

Fig. 7. Fracture toughness and hardness vs penetration load by indentation tests.

effective Young's modulus E_c is 112.40 GPa by the rule of mixtures. The Poisson's ratios of SiO_2 and Al_2O_3 are 0.17 and 0.22, respectively.[20] Therefore the Poisson's ratio of the matrix is assumed to be 0.17–0.22. With those values of particle and matrix, the modulus of LTCC predicted with micromechanics Eqs. (2)–(4) is 100.97–100.98 GPa. Therefore, the calculated E_c by the rule of mixtures agrees well with the experimental results, while the Mori–Tanaka method gives a little smaller value. Taya and Chou[21] compared these two methods for the case of fibers and particles filled materials. When the fillers are only fibers, E_c predicted by Mori–Tanaka method is slightly smaller than that by the rule of mixtures method. Moreover, the E_c value by Mori–Tanaka method decreases with the increase of the particle content and finally to a much smaller value when the fillers are only particles. The effect of particle shape on the mechanical properties is due to the difference of particle surface area and stress distribution in the composites materials.

Therefore, the predictive results by the micromechanics methods and the rule of mixtures are in good coincidence with that by nanoindentation and 3PB tests. Compared with other Refs.,[5,6,9,10] the mechanical properties of the LTCC studied are better than cordierite, many glass–ceramics such as LiO_2–ZrO_2– SiO_2– Al_2O_3 glass–ceramics, and most green tapes such as Dupont 943, Ferro A6 and Heraeus CT2000.

Fig. 6 shows the fracture surface of one LTCC sample by 3PB tests. It is relatively flat, the representing characteristics of brittle fracture. The particles are still embedded in the matrix which means that the interfacial adhesion between the particle and the matrix is good. A few round pores are observed on the fracture surface. From the regular shape of those pores, they are formed during the sintering process. The pores can be controlled by adjusting the sintering temperature and applied pressure load during the processing[10,12].

3.2.3. *Indentation tests for fracture toughness measurement*

In Fig. 7 the variation of the fracture toughness K_{IC} calculated with Eq. (1) and hardness measured by indentation tests under the press load of 5, 10 and 20 N are shown. The K_{IC} values decrease slightly with the increasing load, which was also observed by other researchers and attributed to the use of different calculation equations of K_{IC}.[22] If suitable equation is chosen to characterize the material, the load dependence of K_{IC} can be reduced. The stable hardness values indicate that the applied load is large enough to achieve fully plastic deformation.

The reliability of LTCC devices is highly related to the generation and propagation of the micro-cracks. It is difficult to make

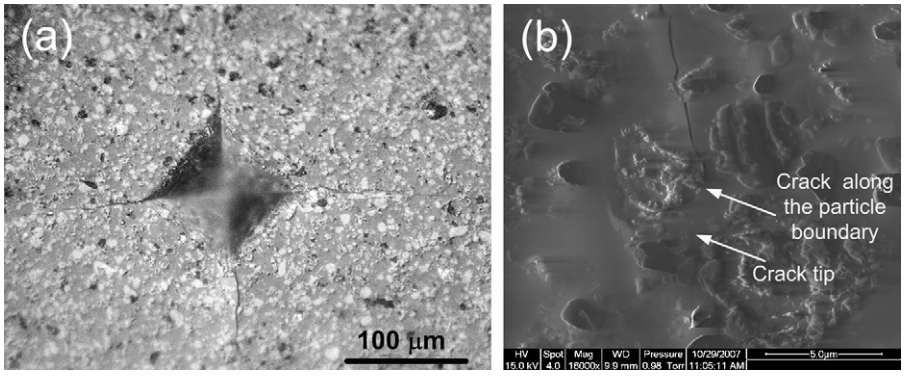

Fig. 8. (a) OM photograph showing indent pit and four extending cracks and (b) SEM photograph showing the crack propagation in the matrix and along the particle boundary.

the notch groove on the LTCC sample because of its brittleness and small thickness, so the indentation test becomes one of the most effective and convenient methods to determine the fracture toughness. The indent pit is clearly observed with four cracks extending from the indent angles, as shown in Fig. 8a. To the typical half penny shaped cracks, Eq. (1) is appropriately used to calculate the fracture toughness.[18] The crack length along four angles may be different due to the difference in local microstructures and residual stress of the surface layer. It is found from the micrograph in Fig. 8b that the crack propagates both in the matrix and along the boundary of the particles. When the crack meets a particle during its propagation, it forces the debonding at the particle–matrix interface and then deviates along the interface. Therefore, the resistance to crack propagation by the particles causes the increase of the fracture toughness. It has been reported that the crack propagation was slowed down with increasing volume fraction of particles and affected as well by the surface energy, particle shape and size as well as the particle–matrix interface.[23,24]

4. Conclusions

By microscopic observation and mechanical tests, the microstructure and mechanical properties of a LTCC have been investigated. The results obtained give the details of microstructure and mechanical behavior as well as their relationship.

The LTCC studied is composed of homogeneously dispersed Al_2O_3 particles and the matrix of mainly Al_2O_3 and SiO_2. The particle has irregular shape with an average radius of 0.71 μm and a volume fraction of about 27%. The adhesion of the particle–matrix interface is found to be strong.

The modulus and hardness of the particles and matrix are successfully determined in mode of modulus mapping of nanoindentation tests. The prediction with the Mori–Tanaka model and the rule of mixtures gives the effective modulus of LTCC, which is in good agreement with the values by 3PB and nanoindentation tests. The fracture toughness of the LTCC studied is obtained and the failure mechanisms by crack propagation both in the matrix and at the interface are revealed.

Acknowledgments

This work is supported by the National High Technology Research and Development program (863 Program) of China (No. 2007AA04Z352) and National Natural Science Foundation of China (No. 60501007). The authors also appreciate CETC No. 43 Research Institute (Hefei, China) which kindly provided the specimens.

References

1. Gongora-Rubio, M. R., Espinoza-Vallejos, P., Sola-Laguna, L. and Santiago-Aviles, J. J., Overview of low temperature co-fired ceramics tape technology for meso-system technology (MsST). *Sens. Actuator A:Phys.*, 2001, **89**, 222–241.
2. Imanaka, Y., *Multilayered Low Temperature Cofired Ceramics (LTCC) Technology*. Springer, Boston, 2005, pp. 2–10.
3. Dernovsek, O., Naeini, A., Preu, G., Wersing, W., Eberstein, M. and Schiller, W. A., LTCC glass–ceramic composites for microwave application. *J. Eur. Ceram. Soc.*, 2001, **21**, 1693–1697.
4. El-Kheshen, A. A. and Zawrah, M. F., Sinterability, microstructure and properties of glass/ceramic composites. *Ceram. Int.*, 2003, **29**, 251–257.
5. Tagami, K., Kubo, T., Makihara, C., Tanahashi, S., Emura, H., Tanaka, J. *et al.*, Glass–ceramics functional substrate development. In *Proceedings of the Sixth International Conference on Multichip Modules*, ed. J. W. Balde, 1997. pp. 363–370.
6. Jones, W. K., Liu, Y., Larsen, B., Wang, P. and Zampino, M., Chemical, structural, and mechanical properties of the LTCC tapes. *Int. J. Microcircuits Electron. Packag.*, 2000, **23**, 469–473.
7. Gongora-Rubio, M., Sola-Laguna, L. M., Moffett, P. J. and Santiago-Aviles, J. J., The utilization of low temperature co-fired ceramics (LTCC-ML) technology for meso-scale EMS, a simple thermistor based flow sensor. *Sens. Actuator A:Phys.*, 1999, **73**, 215–221.
8. Dannheim, H., Schmid, U. and Roosen, A., Lifetime prediction for mechanically stressed low temperature co-fired ceramics. *J. Eur. Ceram. Soc.*, 2004, **24**, 2187–2192.
9. Jantunen, H., *A Novel Low Temperature Co-Firing Ceramic (LTCC) Material for Telecommunication Devices*. Oulu University Press, Oulu, 2001, pp. 15–44.
10. Jung, B. H., Hwang, S. J. and Kim, H. S., Glass–ceramic for low temperature co-fired dielectric ceramic materials based on La_2O_3–B_2O_3–TiO_2 glass with BNT ceramics. *J. Eur. Ceram. Soc.*, 2005, **25**, 3187–3193.
11. Mohanram, A., Lee, S. H., Messing, G. L. and Green, D. J., Constrained sintering of low-temperature co-fired ceramics. *J. Am. Ceram. Soc.*, 2006, **89**, 1923–1929.
12. Ollagnier, J. B., Guillon, O. and Rodel, J., Effect of anisotropic microstructure on the viscous properties of an LTCC material. *J. Am. Ceram. Soc.*, 2007, **90**, 3846–3851.
13. Gomes, C. M., Oliveira, A. P. N., Hotza, D., Travitzky, N. and Greil, P., LZSA Glass–ceramic laminates: fabrication and mechanical properties. *J. Mater. Process. Technol.*, 2008, **206**, 194–201.
14. Hu, T., Uusimaki, A., Jantunen, H., Leppavuori, S., Soponmanee, K. and Sirisoonthorn, S., Optimization of $MgTiO_3$–$CaTiO_3$ based LTCC tapes containing B_2O_3 for use in microwave applications. *Ceram. Int.*, 2005, **31**, 85–93.
15. Lu, A. G. and Qiu, T., Microstructure and properties of calcium borosilicate and borosilicate glass–ceramic composites. *Key Eng. Mater.*, 2008, **368–372**, 1422–1425.
16. Eustice, A. L., Horowitz, S. J., Stewart, J. J., Travis, A. R. and Sawhill, H. T., Low-temperature co-fired ceramics: a new approach to electronic packaging. In *Proceedings of the 36th Electronic Components Conference*, 1986, pp. 37–47.
17. Evans, A. G. and Charles, E. A., Fracture toughness determinations by indentation. *J. Am. Ceram. Soc.*, 1976, **59**, 371–372.
18. Tandon, R., Newton, C. S., Monroe, S. L., Glass, S. J. and Roth, C. J., Subcritical crack growth behavior of a low-temperature co-fired ceramic. *J. Am. Ceram. Soc.*, 2007, **90**, 1527–1533.
19. Weng, G. J., Some elastic properties of reinforced solids with special reference to isotropic ones containing spherical inclusions. *Int. J. Eng. Sci.*, 1984, **22**, 845–856.
20. Schneider, S. J., *Engineered Materials Handbook, Volume 4: Ceramics and Glasses*. ASM International, SAN, 1991, pp.751–755.
21. Taya, M. and Chou, T. W., On two kinds of ellipsoidal inhomogeneities in an infinite elastic body: an application to a hybrid composite. *Int. J. Solids Struct.*, 1981, **17**, 553–563.
22. Ekberg, I. L., Lundberg, R., Warren, R. and Carlsson, R., Indentation testing of SiC-Whisker reinforced Al2O3 composites. In *In Proceedings of the Second International Symposium on Brittle Matrix Composites*, ed. A. M. Bradt, 1988. pp. 84–97.
23. Budiansky, B., Amazigo, J. C. and Evans, A. G., Small-scale crack bridging and the fracture-toughness of particulate-reinforced ceramics. *J. Mech. Phys. Solids.*, 1988, **36**, 167–187.
24. Li, Z., Ghosh, A., Kobayashi, A. S. and Bradt, R. C., Indentation fracture-toughness of sintered silicon-carbide in the palmqvist crack regime. *J. Am. Ceram. Soc.*, 1989, **72**, 904–911.